Journal of Solid State Chemistry **162,** 282–292 (2001)
doi:10.1006/jssc.2001.9294, available online at http://www.idealibrary.com on IDEAL®

Spin State Behavior in Some Cobaltites (III) and (IV) with Perovskite or Related Structure[1]

Michel Pouchard,[2] Antoine Villesuzanne, and Jean-Pierre Doumerc[3]

ICMCB-CNRS, 87, Avenue du Dr. A. Schweitzer, 33608 Pessac, France

Received March 14, 2001; in revised form June 26, 2001; accepted July 2, 2001

IN HONOR OF PROFESSOR PAUL HAGENMULLER ON THE OCCASION OF HIS 80TH BIRTHDAY

The peculiar behaviors of trivalent ($3d^6$) and tetravalent ($3d^5$) cobalt ions coordinated to six oxygen atoms forming a regular or distorted octahedral site are emphasized. Low spin (LS), intermediate spin (IS), and high spin (HS) electronic configurations can be considered for Co^{3+} ($S = 0$, $S = 1$, and $S = 2$) and for Co^{4+} ($S = 1/2$, $S = 3/2$, and $S = 5/2$) depending on the relative magnitude of electronic correlations and crystal field parameters. A simple model including these effects accounts for spin crossover and has led to the derivation of phase diagrams showing the respective stability range of LS, IS, and HS states. Extended Hückel tight-binding and density functional theory–full-potential linearized augmented plane wave calculations were carried out for $TlSr_2CoO_5$ and $SrCoO_3$. Results from both techniques are compared and used to interpret the specific properties of these oxides, which are attributed to the peculiar character of cobalt (III) and (IV). Unlike in molecular compounds where only magnetic and optical properties can be modified, spin transitions (intraatomic electron transfer) can be strongly coupled with metal–insulator transitions in ionocovalent oxides. Spin equilibrium can lead to partly occupied energy bands as nonintegral oxidation state does for mixed valence oxides, and, furthermore, spin state ordering can occur upon cooling in a way similar to charge ordering.

INTRODUCTION

In 1986, the discovery of high T_c superconductivity by Bednorz and Müller (1) gave rise to a renewed interest in ternary or quaternary oxides of 3*d* transition metals and to the discovery of a lot of new families of (II)/(III) mixed valence cuprates, most of them issuing from the first copper (III) perovskites obtained 15 years earlier (2, 3). More recently, the discovery of giant or even colossal magnetoresistive effects for (III)/(IV) mixed valence manganites brought a new development of the works on the oxides of the first transition series such as Co and Ni oxides.

The purpose of the present work is to show the peculiarity of the behavior of cobalt (III) and (IV), the electronic structures of which can exhibit various spin states i.e., low spin (LS), high spin (HS), or intermediate spin (IS) states. Using the case of two recently found cobaltites, $TlSr_2CoO_5$ (Co(III)) (4) and $SrCoO_3$ (Co(IV)) (5–7), we shall discuss the properties and the modeling—using both *ab initio* density functional theory (DFT) and semiempirical extended Hückel tight-binding (EHTB) methods for the electronic structure calculations—of the Co–O bonding as well as the role that this bonding plays regarding the main electronic properties of the relevant oxides.

Overview of the Spin States of d^6 and d^5 Ions

Molecular chemistry is rich in examples where a given ion, generally Fe^{2+} ($3d^6$), exhibits different spin states ($S = 0$, $S = 2$) as the ligands—in most cases linked through a nitrogen atom—are modified. Provided that these ligands are properly chosen, it is possible to observe a progressive (spin equilibrium) or a sharp (spin transition) change between the spin states upon the temperature or pressure influence, or even upon photonic excitation. The cooperative effects can lead to a first-order transition with a hysteresis and hence to bistable systems, appropriate for information storage. For example, see the review papers by Gütlich (8) or Kahn and Martinez (9). For a long time, we have been interested in these phenomena in solid state chemistry of ionocovalent oxides by changing the Fe^{II}–N^{-III} couple for the Co^{III}–O^{-II} one, which is isoelectronic and has a close value of the Dq^* crystal field parameter (10). Especially, we stated that an IS state ($S = 1$) of Co(III) was present in some cobaltites such as La_4LiCoO_8(11) or in

[1] Parts of this article have been presented in an invited talk, entitled "Transition Metal Oxides in the Heart of Modern Solid State Chemistry" at the VIIth European Conference on Solid State Chemistry, Madrid, September 15–18, 1999.

[2] Senior member of the Institut Universitaire de France.

[3] To whom correspondence should be addressed. Fax: 33 5 56 84 83 73. E-mail: doumerc@icmcb.u-bordeaux.fr.

0022-4596/01 $35.00

TABLE 1
Energies of the Various Possible Spin States of a Co^{3+} Ion in O_h Symmetry

$S = 0$	$E_{core} + 3U + 12U' - 6J_H - 24D_q$
$S = 1$	$E_{core} + 2U + 13U' - 7J_H - 14D_q$
$S = 2$	$E_{core} + U + 14U' - 10J_H - 4D_q$

some Co(III)-doped cuprates ($La_4LiCu_{1-x}Co_xO_8$) (12) and that spin transitions could be associated with structural transitions in ternary oxides such as $Sr_2Co_2O_5$ (13). A simple model allowed us to determine the range of the values of the crystal field parameter (Dq) and of the octahedron distortion (θ) for each spin state (14, 15), using modified Tanabe–Sugano diagrams.

Here we propose a more direct approach based on the U and U' interelectronic coulombic repulsion energies and the J_H intraatomic exchange energy, as defined by Kanamori (1963) (16) and more recently by Brandow (1977) (17). Under this formalism, the overall energy of a Co^{3+} ($3d^6$) ion, in O_h symmetry, is given in Table 1 for the various possible spin states. It immediately appears that the IS state is unstable with respect to $S = 0$ and $S = 2$ because if $(U - U') + J_H > 10D_q$ is the condition for stabilizing $S = 1$ with respect to $S = 0$ then $(U - U') + 3J_H > 10Dq$ is also true, which is the condition for stabilizing $S = 2$ with respect to $S = 1$. If we further assume that $(U - U') = 2J_H$ (cf. Appendix 1) these inequalities are reduced to $0.3J_H > Dq$ and $0.5J_H > D_q$, respectively. This limit agrees very well with already proposed values of J_H and D_q($J_H \simeq 0.8$eV (17), $D_q \simeq 2000\ cm^{-1}$ (18)).

However, two factors can modify these conditions:

(i) A large broadening of ionic discrete levels into energy bands, whose width W is proportional to the square of the transfer integral β_{M-O} and inversely proportional to the ionicity E_i (defined as the difference between the Coulomb integrals of the atomic orbitals (AO) of cobalt ($3d$) and oxygen ($2p$)). The mixing of atomic states decreases the U, U', and J_H parameters from the free ion values as the nephelauxetic effect does for the Dq and B parameters in molecular systems. We use atomic d orbital labels for designating the crystalline wave functions Ψ_k resulting from their mixing with O $2p$ and $2s$ orbitals.

(ii) A distortion of the octahedron of either the pyramidal type (C_{4v} symmetry) or the elongated octahedron type (D_{4h} symmetry), which lifts the degeneracy of t_{2g} and e_g levels.

First, we consider the energy of the outer electrons of the metal as a function of the previous parameters, in O_h symmetry (Fig. 1) noticing that, for a perovskite or related structure, the broadest band is of σ_{eg} type ($\beta_\sigma \gg \beta_\pi$). The overlap of the σ^{α}_{eg} and π^{β}_{eg} bands (α and β denote the majority and minority spin projections) results from their broadening and their tendency to get closer.

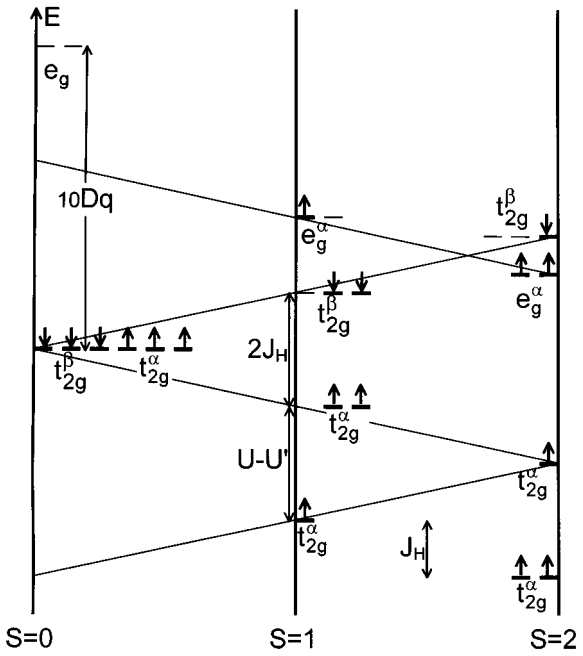

FIG. 1. Energy levels of d electrons for a $3d^6$ configuration in O_h symmetry taking into account exchange (J_H), correlation (U and U'), and crystal field (Dq) parameters.

In a single valence model that could account for metallic *vs* insulating ground state, we must also include additional correlation effects. The position of the upper Hubbard band (UHB) corresponds to the excitation $2Co^{3+} \rightarrow Co^{2+} + Co^{4+}$, i.e., to a $3d^7$ (Co^{2+}) ion, which has two possible configurations, either $t_{2g}^6 e_g^1$ (LS) or $t_{2g}^5 e_g^2$ (HS). For LS Co^{3+}, the d^{n+1} UHBis of the $t_{2g}^6 e_g^1$ type, whereas it is of the $t_{2g}^5 e_g^2$ type for IS or HS Co^{3+}. It can be seen that the gap between the two Hubbard bands is smallest for $S = 1$ (Appendix 2). We conclude that the metallic state is associated with the IS state $t_{2g}^{\alpha 3} t_{2g}^{\beta 2} e_g^{\alpha 1}$. Among various hypotheses, this solution was recently proposed by several authors (19–21) using other arguments.

The role of an octahedron distortion is even more determining for the stabilization of the IS ($S = 1$) state. In an ionic model, the energy of the AO originating from e_g ($d_{x^2-y^2}$:b_{1g}; d_{z^2}:a_{1g}) and from t_{2g}(d_{xz}, d_{yz}:e_g; d_{xy}:b_{2g}) can be given, as for instance by Krishnamurthy and Shaap (22), by tuning the value of the octahedron distortion coefficient k between 0 and 1, with $k = 0$ for a regular octahedron (O_h), $k_{C_{4v}} = 1$ for a fivefold pyramidal coordination, and $k_{D_{4h}} = 1$ for a fourfold square planar coordination. The energy of the outer electrons then varies with U, U', J_H, Dq and k. In this way, Fig. 2 gives the variation of the d orbitals' energy as a function of an increasing C_{4v} distortion from $k = 0$ (six ligands) to $k_{C_{4v}} = 1$(five ligands) and the phase diagram J_H/Dq *vs* k for the three spin states in the usual case where $(U - U') = 2J_H$. Above a critical value $k_c = 0.38$, the IS

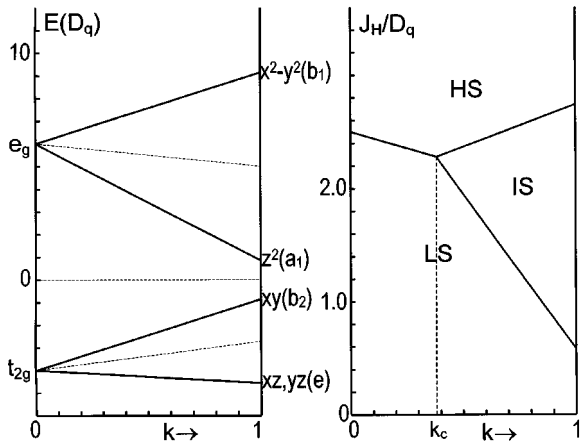

FIG. 2. Orbital energies of a sixfold coordinated $3d^6$ configuration *vs* k in O_h ($k = 0$) and C_{4v} ($0 < k \leq 1$) symmetries (left) and corresponding phase diagram as a function of exchange-correlation (J_H), crystal field (D_q), and distortion (k) parameters (right).

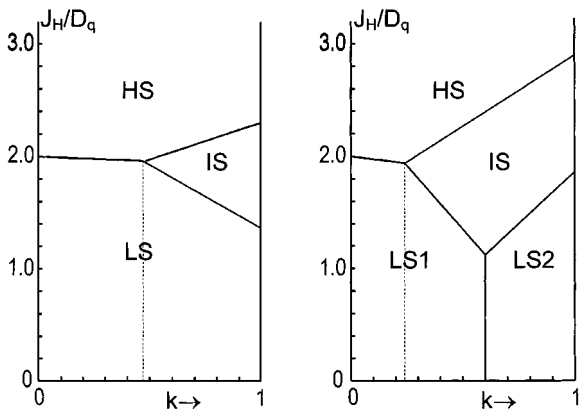

FIG. 4. Phase diagrams for a $3d^5$ configuration in C_{4v} (left) and D_{4h} (right) symmetries as a function of exchange-correlation (J_H), crystal field (D_q), and distortion (k) parameters.

state becomes stable with the following configuration: $d^{\alpha 2}_{xz,yz}$ $d^{\beta 2}_{xz,yz}$ $d^{\alpha 1}_{xy} d^{\alpha 1}_{z^2}$. Figure 3 shows the case of a D_{4h} distortion increasing from a regular octahedron to a square. The diagram shows two critical values for k: a first one that is small (≈ 0.2), and above which the IS state becomes stable in a very broad range of both (J_H/D_q) and k values, and a second one above which the distortion is less stabilizing as the coordination number progressively decreases. The latter corresponds to the crossing of d_{xy} (b_{2g}) and d_{z^2} (a_{1g}) orbitals.

Figure 4 gives similar phase diagrams for Co(IV): $3d^5$ in C_{4v} and D_{4h} symmetries. Here again, the two types of distortions stabilize the IS state, although its existence domains appear to be narrower than those for Co(III).

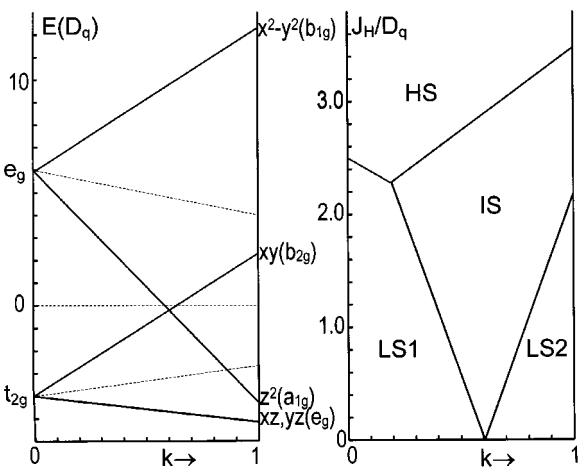

FIG. 3. Orbital energies of a sixfold coordinated $3d^6$ configuration *vs* k in O_h ($k = 0$) and D_{4h} ($0 < k \leq 1$) symmetries (left) and corresponding phase diagram as a function of exchange-correlation (J_H), crystal field (D_q), and distortion (k) parameters (right).

Electronic Structure of the cobaltite (III) $TlSr_2CoO_5$

Some of us recently prepared the cobaltite $TlSr_2CoO_5$ (4, 23), whose high temperature (HT) form is isostructural with the so-called Tl-1201 superconducting cuprate (space group, $P4/mmm$) of formula $TlSr_{2-x}La_xCuO_5$. We searched for stabilizing the IS state of Co(III) thanks to an octahedron distortion as large as possible—the Tl-1201 cuprate exhibits the highest octahedron elongation—and to a wide $\sigma_{x^2-y^2}$ band resulting from the shortest equatorial Co–O distances.

Actually, in this HT form the D_{4h} symmetry of the octahedron is characterized by a strong distortion with apical Co–O distances of 2.34 Å *vs* equatorial Co–O distances of 1.87 Å. We have shown that, above 310 K, the oxide is an *n* type metal with strong ferromagnetic interactions (24). At low temperature (LT), a commensurate modulation leads to an orthorhombic cell ($a\sqrt{2}$, $3a\sqrt{2}$, $2c$; space group, *Cmcm*) containing two well-differentiated sites for Co ions (23). The Co1 site has a symmetry close to that of D_{4h} with a strong shortening of equatorial Co–O distances ($d'' = 2.17$ Å; $d^{\perp} = 1.79$ Å). The Co2 site has a symmetry close to that of C_{4v} with five Co–O distances ranging from 1.89 to 2.01 Å, the sixth one being of 2.47 Å. The LT phase is insulating and becomes antiferromagnetic below 150 K (25).

Modeling the HT phase. A Mössbauer study (26) of a lightly ^{57}Fe-doped sample clearly reveals two well-separated quadrupolar doublets, which suggests a dynamic phase separation on a nanometric scale, as it is not seen using classical X-ray or electron diffraction. X-ray synchrotron or

TABLE 2
AO Parameters for EHTB Calculations: Ionization Energies H_{ii} and ζ Exponents in Slater-Type Expression

	Tl		Sr		Co			O	
Orbital:	6*s*	6*p*	5*s*	5*p*	4*s*	4*p*	3*d*	2*s*	2*p*
H_{ii} (eV)	− 11.60	− 5.80	− 6.62	− 3.92	− 9.21	− 5.29	− 13.18	− 32.3	− 14.8
ζ	2.30	1.60	1.214	1.214	2.0	2.0	5.55 (0.56786) 2.10 (0.60586)	2.275	2.275

Note. Coefficients for double ζ expansions are shown in parentheses.

X-ray absorption should carry additional evidences of this dynamic phase separation.

Band structure calculations were performed using the semiempirical extended Hückel tight-binding (EHTB) method (27), implemented in the CAESAR package (28), with parameters given in Table 2. EHTB calculations confirm—only taking into account orbital overlaps—that *d* bands are no longer degenerate (Fig. 5), in agreement with the above ionic model. A $\sigma^*_{x^2-y^2}$ band is shifted upward by nearly 2.5 eV with respect to $\sigma^*_{z^2}$, the splitting being less important for the bands arising from t_{2g}. The $\sigma^*_{x^2-y^2}$ band should in principle remain empty, which would agree with our hypothesis of an IS state.

To take into account correlation effects that are not included in the EHTB method, we propose to apply empirically evaluated corrections to this model for the various contributions: $(U - U' - \delta)$ for $\pi^{\alpha}_{xz,yz}$ with respect to π^{α}_{xy} (δ is the crystal field splitting of d_{xy} *vs* d_{xz}, d_{yz} orbitals) and $2J_H$ for $\pi^{\beta}_{xz,yz}$ with respect to $\pi^{\alpha}_{xz,yz}$. Knowing that $U - U' = 2J_H$ and in view of the 2.5-eV separation between $\pi_{xz,yz}$ and $\sigma^*_{x^2-y^2}$ in the uncorrelated case, the vicinity of $\pi^{\beta}_{xz,yz}$ and $\sigma^{\alpha*}_{x^2-y^2}$ results from a very reasonable value of *ca.* 0.6 eV for J_H (Fig. 6). Under such conditions, a spin equilibrium IS↔HS should occur at increasing temperature. The $\pi^{\beta}_{xz,yz}$ electron belonging to a π antibonding band, and hence rather localized, is transferred into a broader $\sigma^{\alpha*}_{x^2-y^2}$ band and therefore should become itinerant. However, this electron remains attracted by the localized hole created in the $\pi^{\beta}_{xz,yz}$ band, and it forms a polaron that favors the ferromagnetic coupling of the surrounding localized spins. The metallic phase cannot grow much as the $\sigma^{\alpha*}_{x^2-y^2}$ electron occupies an antibonding σ state leading to an expansion of the Co–O equatorial bonds compensated by an equatorial compression of neighboring cells, which tends to prevent a further growing of the new phase. This model explains the existence of two different sites for ^{57}Fe atoms observed by Mössbauer spectroscopy.

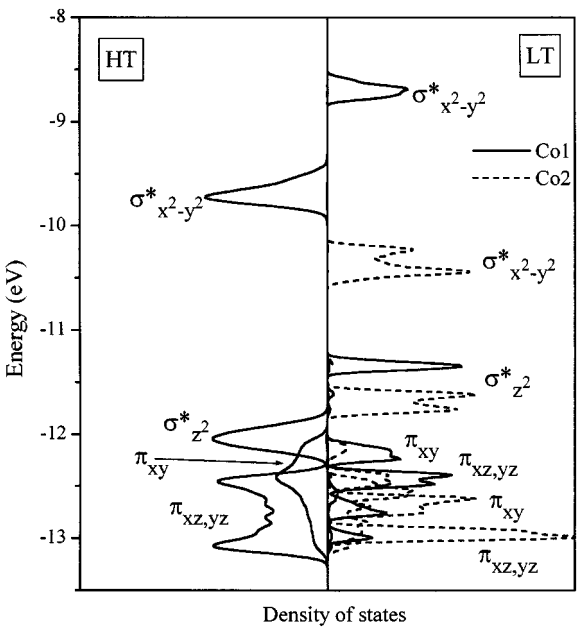

FIG. 5. EHTB calculations for $TlSr_2CoO_5$. DOS curves for the HT and LT phases.

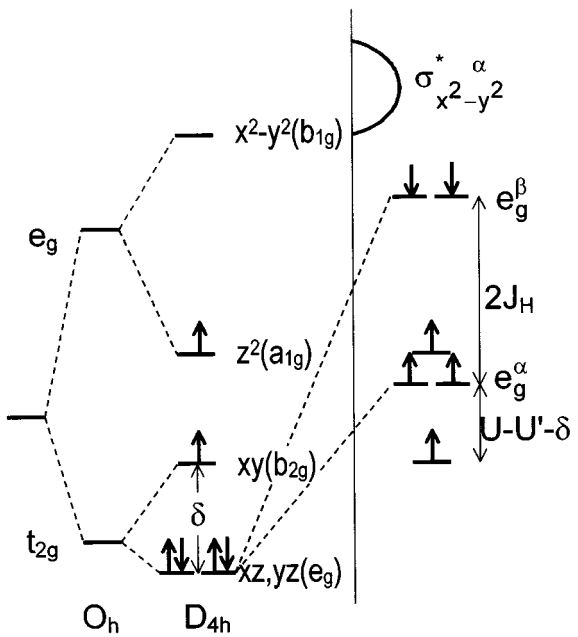

FIG. 6. Correlation effects for the HT form of $TlSr_2CoO_5$.

After a time that must be longer than the characteristic time of Mössbauer spectroscopy, i.e., $\sim 10^{-7}$ s, the spin equilibrium brings back the $\sigma^{*}_{x^2-y^2}$ electron into its $\pi^{\beta}_{xz,yz}$ hole. The modified domain becomes insulating again and another IS $\leftrightarrow$HS transition can take place nearby. It is only when the rate of metallic phase reaches the percolation threshold that the sample becomes metallic on a macroscopic scale.

More sophisticated calculations, in the framework of the DFT (29) were carried out. We used the full-potential linearized augmented plane wave method (FLAPW) (30), under the Local Density Approximation (LDA) for the exchange-correlation energy (31), implemented in the WIEN97 code (32). We used atomic positions and crystal parameters from experiments (23); muffin-tin radii of 2.2 bohr for Tl, 2.15 bohr for Sr, 1.89 bohr for Co, and 1.65 bohr for O; a basis set of about 1120 plane waves; and a regular mesh of 1000 k-points to carry out Brillouin zone integrations (i.e., 84 k-points in the irreducible Brillouin zone (IBZ)).

Our results agree with those obtained recently by Foerster *et al.* (33) with the aid of the full-potential nonorthogonal local orbital method (FPLO). A spin-polarized calculation led to an energy lower by 0.52 eV per unit cell with respect to a nonmagnetic calculation, which well accounts for the ferromagnetic interactions characteristic of the metallic phase. The stabilization of a magnetic phase is consistent with the very high density of states at the Fermi level (E_F) found in the nonmagnetic calculation (Stoner instability). The difference between majority α and minority β spins gives nearly 1.93 μ_B per cobalt atom and 0.63 μ_B shared mainly by oxygen atoms belonging to the CoO_2 equatorial plane. Here again these calculations agree with the proposed spin equilibrium between IS ($S = 1$, 2 μ_B) and HS ($S = 2$, 4 μ_B) and the high temperature susceptibility data leading to a Curie constant, the value of which ($C = 1.7$) is between those expected for an IS state ($C_{IS} = 1$) and an HS state ($C_{HS} = 3$). Figures 7 and 8 give density of state (DOS) curves for majority and minority spins, projected on various cobalt AO and oxygen sites. It appears that each d orbital of cobalt contributes significantly to its magnetic moment.

There are three different oxygen sites in $TlSr_2CoO_5$: O1, O2, and O3 correspond to apical, TlO and CoO_2 layers, respectively. Co and O3 alone contribute to states crossing E_F, leading to the net moment carried by O3 and to the two-dimensional character of electric and magnetic properties for $TlSr_2CoO_5$. As a matter of fact, O1 and O2 partial

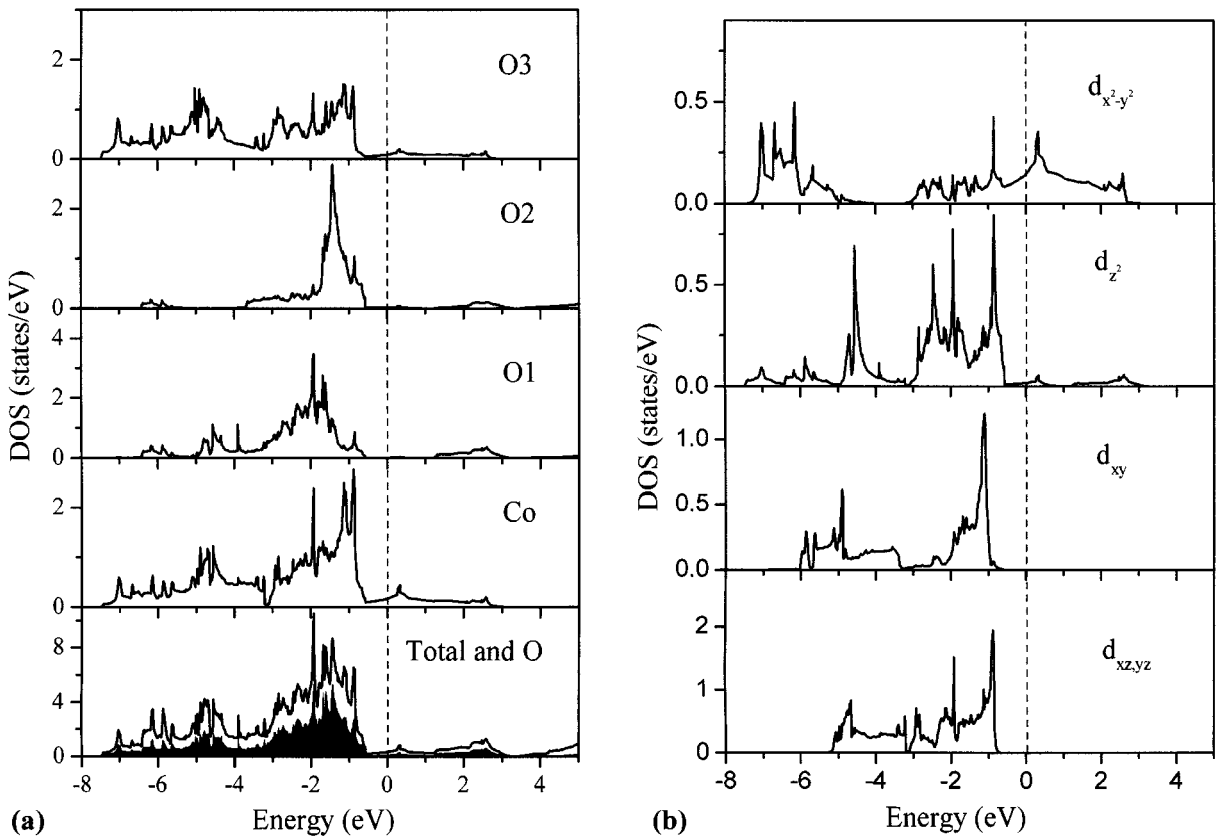

FIG. 7. FLAPW calculations. Total and partial DOS for majority spins in $TlSr_2CoO_5$ with contributions from cobalt and oxygen sites (a) and from cobalt 3d orbitals (b). Dashed line is the Fermi level.

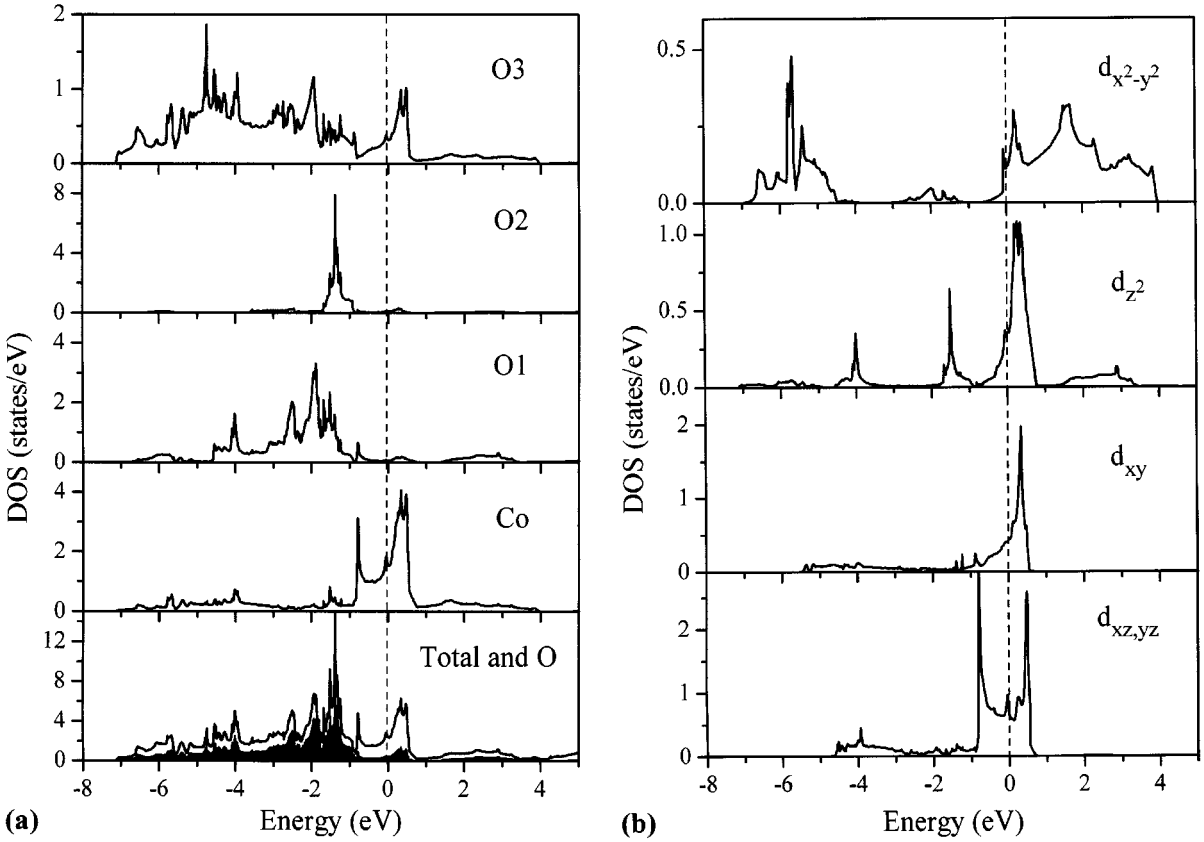

FIG. 8. FLAPW calculations. Total and partial DOS for minority spins in $TlSr_2CoO_5$ with contributions from cobalt and oxygen sites (a) and from cobalt 3*d* orbitals (b). Dashed line is the Fermi level.

DOS values for majority and minority spins are almost similar and lie at the same energy.

For majority spins, the Fermi level E_F lies in the $\sigma^*_{x^2-y^2}$ band, whose large width accounts for the metallic character of the HT phase. It is noticeable that, according to its σa_{1g} symmetry, the Co d_{z^2} orbital also takes part in this band. The increasing DOS *vs* energy for $E > E_F$ is in good agreement with the *n* type conductivity revealed by a negative value of thermopower (24). Figure 8 shows that an usual electronic structure is obtained for minority spins, i.e., involving states of dominant cobalt character in the vicinity and above E_F and states of oxygen character lying at lower energies (up to 1 eV below E_F). On the contrary, Fig. 7 shows that, for majority spins, all represented bands (on a more than 10-eV-wide range around E_F) have an almost perfect mixed cobalt–oxygen character, corresponding to a much more covalent bonding.

Summing over all occupied states of the Brillouin zone leads to an ionic charge on cobalt of about + 2.5. As the empty states located above E_F do not correspond to pure oxygen states, but to mixed Co–O3 states, the holes on oxygen atoms must be considered as resulting from the covalency rather than from the formation of stable O(-I) states.

EHTB Modeling of the Low Temperature Phase. Figure 5 gives the DOS curves for the orthorhombic cell of the LT phase. Comparing the LT phase with the HT phase clearly shows that the two cobalt sites are also well differentiated in the energy diagram, notably concerning the $\sigma^*_{x^2-y^2}$ bands. This allows us to ascribe an IS configuration to Co1 and an HS configuration to Co2 as sketched in Fig. 9 where monoelectronic diagrams account for the site symmetry and size, and correlation effects are taken into account using empirically determined U, U', and J_H parameters. In this perspective, we can predict a magnetic structure analogous to the stripe structures found for cuprates, nickelates, and manganites (34). Interactions between empty $\sigma^*_{x^2-y^2}$ (Co1) and half-occupied $\sigma^*_{x^2-y^2}$ (Co2) orbitals are ferromagnetic; on the other hand, $\sigma^*_{x^2-y^2}$(Co2)–$\sigma^*_{x^2-y^2}$(Co2′) interactions are antiferromagnetic. Therefore the magnetic ordering should correspond to ferromagnetic triple chains along the [110] direction of the tetragonal subcell, antiferromagnetically coupled with each other (Fig. 10).

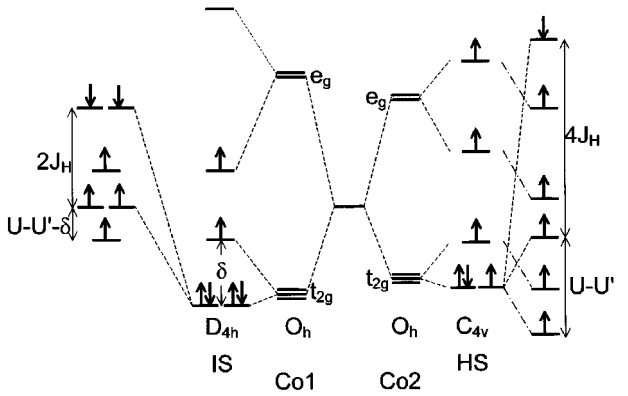

FIG. 9. Splitting of energy levels in Co1 and Co2 sites of the LT form of $TlSr_2CoO_5$. Dash-dotted lines for Co2 show the stabilization by J_H due to the $t_{2g}^{\beta} \rightarrow e_g^{\alpha}$ (IS $\rightarrow$ HS) electron transfer.

A neutron diffraction study is in progress to check this hypothesis.

As a conclusion, we can say that a spin equilibrium takes place in the HT phase that freezes or "disproportionates" at low temperature, giving rise to a spin state ordering (SSO) with one third of cobalt atoms in an IS state and two thirds in an HS state. Actually, this transition corresponds to a volume decrease as T increases. It represents a new type of transition that in some way recalls charge-ordering triggered reactions of the type found in mixed valence GMR manganites. In fact, the filling of the $\sigma^*_{x^2-y^2}$ band here no longer depends on the doping as in the $Sr_{1-x}Ln_xMnO_3$ phases, but on the spin equilibrium that is controlled by temperature and pressure conditions, as well as probably by interaction with photons of matching energy. We shall develop our present investigations to check whether some effects such as the light-induced excited spin state trapping (LIESST effect) (35, 36) occurs in these cobaltites.

Electronic Structure of the Cobaltite (IV) $SrCoO_3$

$SrCoO_3$ has a perovskite type structure belonging to the space group *Pn3m*. It was synthesized under high oxygen pressures (37). Some of us recently obtained it at room temperature and pressure using oxygen electrochemical intercalation into the brownmillerite oxide $Sr_2Co_2O_5$ (5). $SrCoO_3$ is a *n* type ferromagnetic metal up to *ca.* 300 K with a magnetic moment of 2.1 μ_B as deduced from magnetization curves at low temperatures. The $3d^5$ configuration of Co^{4+} can also lead to three possible spin states, $S = 1/2$, $S = 3/2$, and $S = 5/2$ (14, 38), the energy of which are recalled in Table 3 for an O_h symmetry. As for the IS ($S = 1$) state of Co(III) the IS ($S = 3/2$) configuration of Co(IV) is not stable *vs* the LS or HS ones.

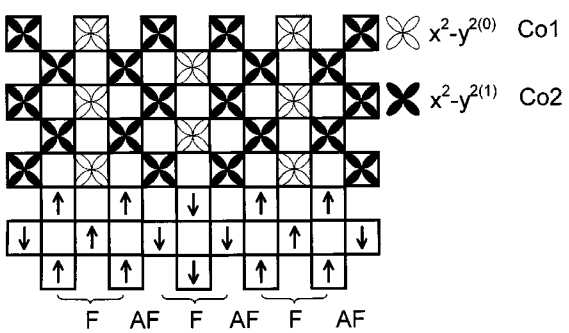

FIG. 10. Predicted magnetic structure for $TlSr_2CoO_5$ below 150 K.

TABLE 3
Energies of the Various Possible Spin States of a Co^{4+} Ion on O_h Symmetry

$S = 1/2$	$E_{core} + 2U + 8U' - 4J_H - 20D_q$
$S = 3/2$	$E_{core} + U + 9U' - 6J_H - 10D_q$
$S = 5/2$	$E_{core} + 10U' - 10J_H$

The diagram taking into account the correlation energies U, U', and J_H for the three spin states is given in Fig. 11, which again shows that the crossing of e_g^{α} and t_{2g}^{β} levels should take place in the vicinity of $S = 3/2$. The prevailing broadening of the σ_{eg}^{α} band indicates that the metallic state should be associated with the IS configuration (Appendix 3) (39, 40). A simple EHTB calculation, with the same parameters as stated previously (Table 2), leads to the DOS curves given in Fig. 12. If one applies to this monoelectronic diagram empirically chosen U, U', and J_H correlation

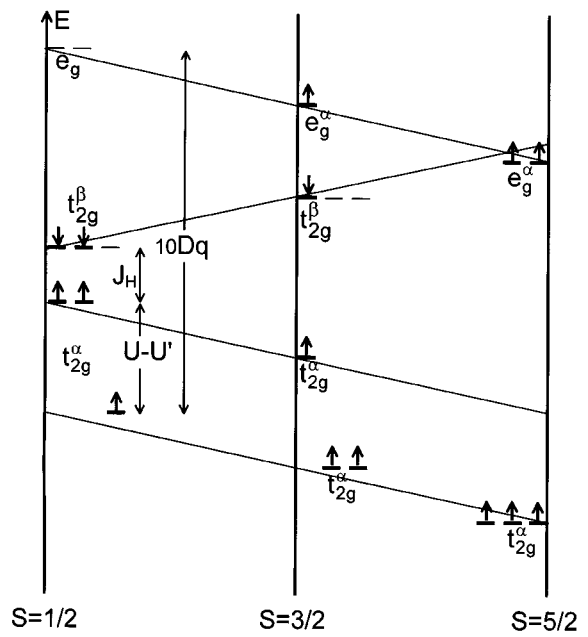

FIG. 11. Energy levels of *d* electrons for a $3d^5$ configuration taking into account exchange (J_H) and correlation (U and U') parameters.

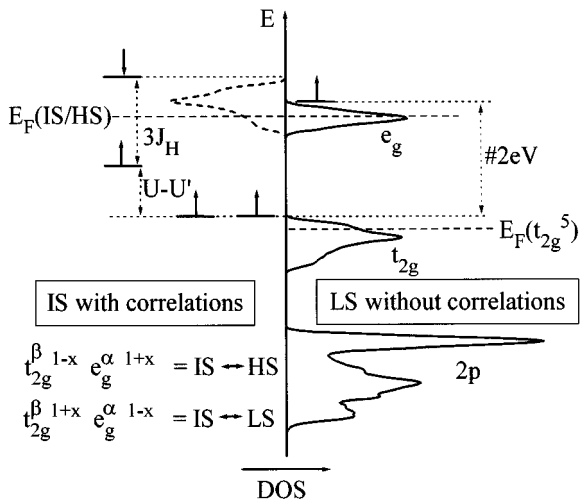

FIG. 12. DOS derived from an EHTB calculation and including the effect of empirically chosen values of exchange and correlation parameters for $SrCoO_3$.

parameters, with values slightly smaller than those previously proposed for $TlSr_2CoO_5$ (Co(III)) and corresponding to the covalency increase of the Co–O bond as Co(III) is replaced by Co(IV) ($J_H \sim 0.4$ eV), it can be predicted that the $\sigma^{\alpha}_{e_g}$ and $\pi^{\beta}_{t_{2g}}$ bands will overlap at the Fermi level. This corresponds to some electron transfer between t^{β}_{2g} and $\sigma^{\alpha}_{e_g}$ or, in other words, to either IS↔HS or IS↔LS spin equilibria. As the Coulomb repulsion with ligands is larger for e_g than for t_{2g} orbitals, like previously, the transfer is limited by the loss of elastic energy.

A first-principles study of $SrCoO_3$ has been carried out using the same FLAPW/LDA method as mentioned previously. We used the experimentally determined cubic unit cell ($a = 3.85$ Å) (5); muffin-tin radii of 2.0 bohr for Sr, 1.9 bohr for Co, and 1.7 bohr for O; a 207 plane waves basis set; and 1000 k-point regular mesh for Brillouin zone integrations (i.e., 56 k-points in the IBZ).

Nonmagnetic calculations give a strong DOS peak at E_F (Stoner instability), of t_{2g} character; as shown in Fig. 13, spin-polarized calculations confirm the ferromagnetic character of $SrCoO_3$ with a magnetic moment of 1.83 μ_B on the cobalt and of 0.19 μ_B on each oxygen atom, in agreement with the experimental data (2.1 μ_B) (5) and some LS↔IS equilibrium. The moment carried by cobalt is due to both e_g and t_{2g} contributions. The magnetic solution has an energy 0.44 eV/unit cell lower than that of the nonmagnetic one. These results are in excellent agreement with those of a previous DFT investigation of $SrCoO_3$ based on the augmented spherical wave method (41).

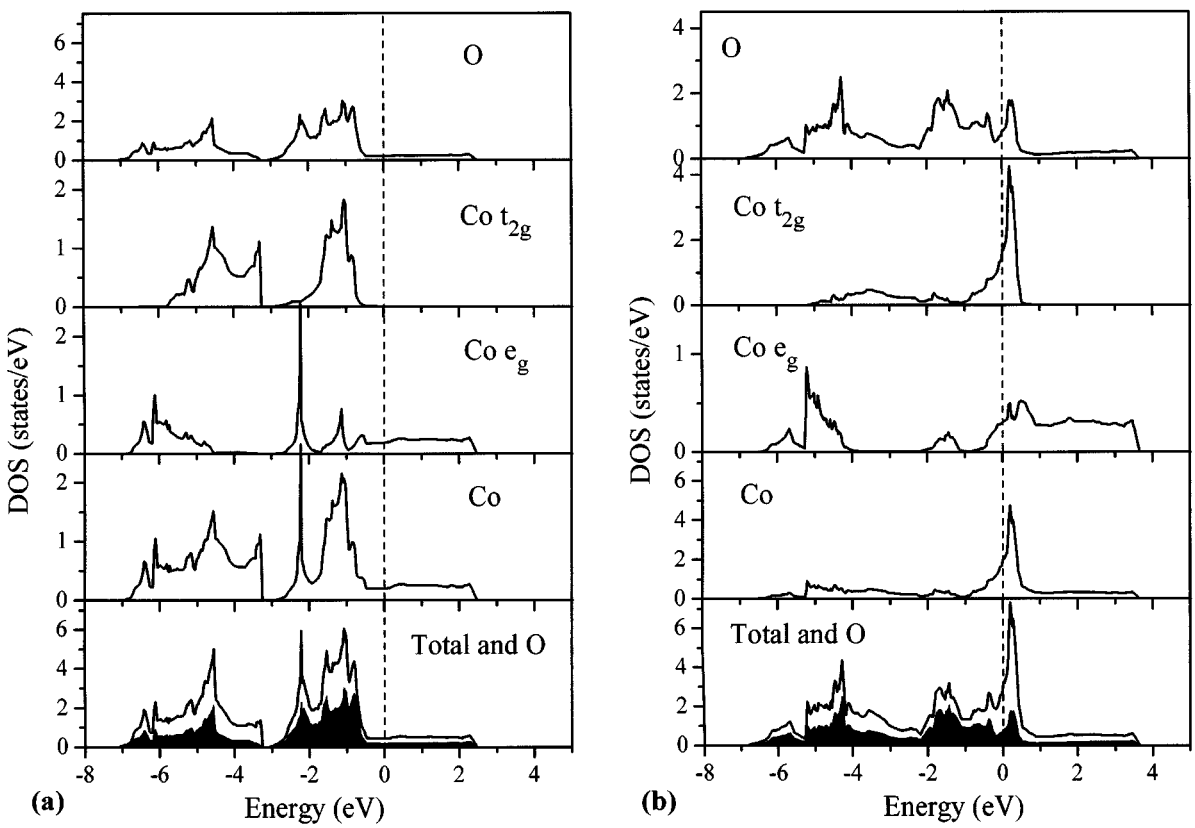

FIG. 13. FLAPW calculations. DOS for $SrCoO_3$ for majority (a) and minority (b) spins.

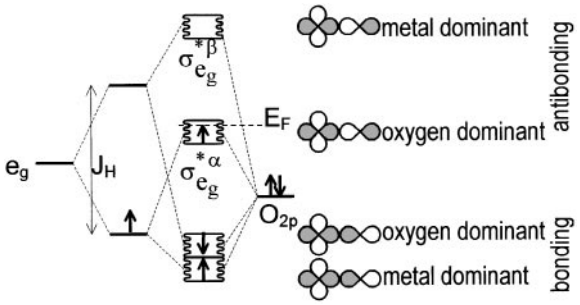

FIG. 14. Reinforcement of oxygen contribution to the $\sigma^{\alpha *}_{e_g}$ band through the effect of the exchange energy.

As is generally observed for this type of calculation, bands are broad and strongly overlap each other. Particularly, one sees that partly occupied majority-spin σ^{α}_{eg} bands have a strong oxygen character. Such a behavior can be easily explained provided that one considers that the majority and minority spin states are separated by an intraatomic exchange energy difference ΔJ_H (Fig. 14) that reinforces the oxygen contribution to the antibonding $\sigma^{\alpha}_{e_g}$ bands even if an average over the two spin orientations results in a rather metallic character. As a general picture, and in the same way as in the case of $TlSr_2Co(III)O_5$, the oxygen contribution to 3*d* character bands is much larger than expected from the classical ionocovalent picture for transition metal oxides. This effect is emphasized for majority spins (Fig. 13), for which Co partial DOS even dominates the oxygen one in low-lying 2*p* character bands (from -3 to -7eV below E_F).

Despite these effects, empty states lying above the Fermi level cannot be viewed as pure holes that could be formulated as O(-I).

CONCLUSIONS

As a conclusion, the exceptional role of cobalt among the 3*d* transition elements can be emphasized regarding the variety of its possible spin states between which equilibria or transitions can be triggered by temperature or pressure changes. Contrasting with molecular compounds where only magnetic and optic local properties can be modified, spin transitions can lead to insulator–metal transitions in nonmolecular two and three-dimensional solids, through electron transfers from localized states, typically of t_{2g} type, into collective states, typically of e_g type. Such a behavior could be at the origin of the unusually large thermal expansion coefficients observed for cobaltites used as cathode in Solid oxide fuel cells (SOFC) (42).

The $t_{2g} \rightarrow e_g$ transfer can lead to ferromagnetic interactions (so-called indirect interactions). The electronic occupancies of the bands can be changed with temperature, in a way equivalent to that of heterovalent substitutions of the large ions in the perovskite-type mixed valence materials such as superconducting cuprates or GMR manganites.

In the cobaltites, the strong covalency of the Co–O bonds that results from the vicinity of the energies of 3*d* (Co) and 2*p* (O) orbitals yields large bandwidths, especially for σ bands, which stabilize IS states that are never stable for molecular species of O_h symmetry.

Modeling the chemical bond and electronic structure with methods as different as those based on tight-binding or on DFT approaches is particularly interesting as each of them has opposed tendencies to either amplify or reduce the value of basic quantities such as band gaps or bandwidths. In the case of EHTB, taking into account U, U', and J_H correlation energies as they are defined by Kanamori (16) and Brandow (17) allows us to account for electronic properties of cobaltites such as $TlSr_2CoO_5$, even if bandwidths are underevaluated. Associated with a structural determination of the HT and LT forms and a Mössbauer study, it allows us to propose an IS–HS equilibrium that gives rise to ferromagnetic polarons, the percolation of which leads to the metallic character of the HT phase and, at LT, a frozen long-range ordering of Co^{3+} IS and HS states (in the ratio 1 to 2) in an antiferromagnetic insulating phase. Such a situation is somewhat analogous to the localization and charge ordering occurring in some GMR manganites at LT. In the case of FLAPW–LDA, directly taking into account correlation effects allows a correct description of the ferromagnetic interactions and a description of empty O 2*p* states as covalency holes lying in bands with mainly a metallic character, but including an amazingly large oxygen contribution thanks to their majority spin character as they are lowered by the exchange energy.

ACKNOWLEDGMENTS

The authors acknowledge the M3PEC Project (Modélisation Microscopique et Mésoscopique en Physique, dans l'Environnement et en Chimie), Université de Bordeaux I, for computational facilities.

APPENDIX 1

According to Kanamori (16) and Brandow (17)

$$U = \langle \mu\mu | \mathrm{V} | \mu\mu \rangle$$

$$U' = \langle \mu\mu' | \mathrm{V} | \mu\mu' \rangle$$

$$J_H = \langle \mu\mu' | \mathrm{V} | \mu'\mu \rangle,$$

where μ and μ' are spatially different 3*d* orbitals on a single site and V is the coulombic operator.

U, U', and J_H are related to Racah parameters A, B, and C according to

$$U = A + 4B + 3C$$

$$U' = A - B + C$$

$$J_H = 5/2B + C,$$

implying $U - U' = 2J_H$.

APPENDIX 2

$S = 0$: $t_{2g}^{\alpha,\beta}(Co^{3+})_{LS} \rightarrow e_g^{\alpha}(Co^{2+})_{LS}$

$$\begin{aligned} Gap^0 &= E(Co^{2+}) - E(Co^{3+}) \\ &= 6U' - 3J_H + 6D_q - (U + 4U' \\ &\quad - 2J_H - 4D_q) - W_\sigma \\ &= U' - 3J_H + 10D_q - W_\sigma, \end{aligned}$$

where W_σ is the σ_{e_g} band width.

$S = 1$: $t_{2g}^{\beta}(Co^{3+})_{IS} \rightarrow e_g^{\alpha}(Co^{2+})_{HS}$ or (′) $e_g^{\alpha}(Co^{3+})_{IS} \rightarrow e_g^{\alpha}(Co^{2+})_{HS}$

$$\begin{aligned} Gap^1 &= 6U' - 4J_H + 6D_q \\ &\quad - (U + 4U' - J_H - 4D_q) - W_\sigma \\ &= U' - 5J_H + 10D_q - W_\sigma \end{aligned}$$

$$\begin{aligned} Gap^{1'} &= 6U' - 4J_H + 6D_q \\ &\quad - (5U' - 3J_H + 6D_q) - W_\sigma \\ &= U' - J_H - W_\sigma \end{aligned}$$

$S = 2$: $t_{2g}^{\beta}(Co^{3+})_{HS} \rightarrow t_{2g}^{\beta}(Co^{2+})_{HS}$

$$\begin{aligned} Gap^2 &= U + 5U' - J_H - 4D_q \\ &\quad - (U + 4U' - 4D_q) - W_\pi \\ &= U' - J_H - W_\pi, \text{ with } W_\pi < W_\sigma. \end{aligned}$$

APPENDIX 3

$S = 1/2$: $t_{2g}^{\beta}(Co^{4+})_{LS} \rightarrow t_{2g}^{\beta}(Co^{3+})_{LS}$

$$\begin{aligned} Gap^{1/2} &= E(Co^{3+}) - E(Co^{4+}) \\ &= U + 4U' - 2J_H - 4D_q \\ &\quad - (U + 3U' - J_H - 4D_q) - W_\pi \\ &= U' - J_H - W_\pi \end{aligned}$$

$S = 3/2$: $t_{2g}^{\beta}(Co^{4+})_{IS} \rightarrow e_g^{\alpha}(Co^{3+})_{HS}$ or (′) $e_g^{\alpha}(Co^{4+})_{IS} \rightarrow e_g^{\alpha}(Co^{3+})_{HS}$

$$\begin{aligned} Gap^{3/2} &= 5U' - 4J_H + 6D_q \\ &\quad - (U + 3U' - 4D_q) - W_\sigma \\ &= U' - 2J_H + 10D_q - W_\sigma \end{aligned}$$

$$\begin{aligned} Gap^{3/2'} &= 5U' - 4J_H + 6D_q \\ &\quad - (4U' - 3J_H + 6D_q) - W_\sigma \\ &= U' - J_H - W_\sigma \end{aligned}$$

$S = 5/2$: $e_g^{\alpha}(Co^{4+})_{HS} \rightarrow t_{2g}^{\beta}(Co^{3+})_{HS}$

$$\begin{aligned} Gap^{5/2} &= U + 4U' - 4D_q \\ &\quad - (4U' - 4J_H + 6D_q) - W_\pi \\ &= U + 4J_H - 10D_q - W_\pi \end{aligned}$$

REFERENCES

1. J. G. Bednorz and K. A. Müller, *Z. Phys. B* **64,** 189 (1986).
2. G. Demazeau, C. Parent, M. Pouchard, and P. Hagenmuller, *Mater. Res. Bull.* **7,** 913 (1972).
3. J. B. Goodenough, G. Demazeau, M. Pouchard, and P. Hagenmuller, *J. Solid State Chem.* **8,** 325 (1973).
4. M. Coutanceau, J. P. Doumerc, J. C. Grenier, P. Maestro, M. Pouchard, and T. Seguelong, *C. R. Acad. Sci. Paris Ser. IIc* **320,** 675 (1995).
5. P. Bezdicka, A. Wattiaux, J. C. Grenier, M. Pouchard, and P. Hagenmuller, *Z. Anorg. Allg. Chem.* **619,** 7 (1993).
6. P. Bezdicka, L. Fournès, A. Wattiaux, J. C. Grenier, and M. Pouchard, *J. Solid State Chem.* **91,** 501 (1994).
7. L. Fournès, A. Wattiaux, A. Demourgues, P. Bezdicka, J. C. Grenier, M. Pouchard, and J. Etourneau, *J. Phys. IV* **7,** C1-353 (1997).
8. P. Gütlich, *Struct. Bonding* **44,** 83 (1981).
9. O. Kahn and C. J. Martinez, *Science* **279,** 44 (1998).
10. M. Pouchard, *in* "IIIrd European Conference on Solid State Chemistry, Regensburg," Vol. 3, p. 412, 1986.
11. G. Demazeau, M. Pouchard, M. Thomas, J. F. Colombet, J. C. Grenier, L. Fournès, J. L. Soubeyroux, and P. Hagenmuller, *Mater. Res. Bull.* **15,** 461 (1980).
12. B. Buffat, G. Demazeau, M. Pouchard, and P. Hagenmuller, *Mater. Res. Bull.* **18,** 1153 (1983).
13. J. C. Grenier, L. Fournès, M. Pouchard, and P. Hagenmuller, *Mater. Res. Bull.* **21,** 441 (1986).
14. B. Buffat, G. Demazeau, M. Pouchard, and P. Hagenmuller, *Proc. Indian Acad. Sci.* **93,** 313 (1984).
15. B. Buffat, G. Demazeau, M. Pouchard, and P. Hagenmuller, Catane, *Atti. Accad. Mediterranea Sci.* **1**(Suppl. 1), 71 (1984).
16. J. Kanamori, *J. Phys. Chem. Solids* **10,** 87 (1963).
17. B. J. Brandow, *Adv. Phys.* **26,** 651 (1977).
18. J. E. Huheey, "Inorganic Chemistry," Harper & Row, New York, 1978.
19. M. A. Señaris-Rodriguez and J. B. Goodenough, *J. Solid State Chem.* **116,** 224 (1995).
20. M. A. Korotin, S. Yu, Ezhov, I. V. Solovyev, and V. I. Anisimov, D. I. Khomskii, and G. A. Sawatzky, *Phys. Rev. B* **54,** 5309 (1996).
21. L. Barbey, N. Nguyen, V. Caegnaert, F. Studer, and B. Raveau, *J. Solid State Chem.* **112,** 148 (1994).
22. R. Krishnamurthy and S. W. Shaap, *J. Chem. Educ.* **46,** 799 (1969).
23. J. P. Doumerc, M. Coutanceau, A. Demourgues, E. Elkaim, J. C. Grenier, and M. Pouchard, *J. Mater. Chem.* **11,** 78–85 (2001).
24. M. Coutanceau, P. Dordor, J. P. Doumerc, J. C. Grenier, P. Maestro, M. Pouchard, D. Sedmidubsky, and T. Seguelong, *Solid State Commun.* **96,** 569–572 (1995).

25. J. P. Doumerc, J. C. Grenier, P. Hagenmuller, M. Pouchard, and A. Villesuzanne, *J. Solid State Chem.* **147,** 211–217 (1999).
26. J. P. Doumerc, M. Coutanceau, L. Fournès, J. C. Grenier, M. Pouchard, and A. Wattiaux, *C. R. Acad. Sci. Paris Ser. IIc*, **2,** 637–643 (1999).
27. R. Hoffmann, *J. Chem. Phys.* **39,** 1397 (1963); J. H. Ammeter, H. B. Bürgi, J. C. Thibeault, and R. Hoffmann, *J. Am. Chem. Soc.* **100,** 3686 (1978); M. H. Whangbo and R. Hoffmann, *J. Am. Chem. Soc.* **100,** 6093 (1978).
28. J. Ren, W. Liang, and M. H. Whangbo, CAESAR package (1998), http://www.primec.com.
29. P. Hohenberg and W. Kohn, *Phys. Rev. B* **136,** 864 (1964); W. Kohn and L. J. Sham, *Phys. Rev. A* **140,** 1133 (1965).
30. O. K. Andersen, *Phys. Rev. B* **12,** 3060 (1975); S. H. Wei and H. Krakauer, *Phys. Rev. Lett.* **55,** 1200 (1985); D. Singh, "Planewaves, Pseudopotentials and the LAPW Method," Kluwer Academic, Boston, 1994, and reference therein.
31. J. P. Perdew and Y. Wang, *Phys. Rev. B* **45,** 13244 (1992).
32. P. Blaha, K. Schwarz, and J. Luitz, WIEN97, A Full Potential Linearized Augmented Plane Wave Package for Calculating Crystal Properties, Karlheinz Schwarz, Techn. Univ. Wien, Vienna, 1999, ISBN 3-9501031-0-4; updated version of P. Blaha, K. Schwarz, P. Sorantin, and S. B. Trickey, *Comp. Phys. Commun.* **59,** 399 (1990).
33. D. Foerster, R. Hayn, T. Pruschke, M. Zölfl, and H. Rosner, arXiv:cond-mat/0010239, http://arXiv.org.
34. J. H. Tranquata, B. J. Sternlieb, J. D. Axe, Y. Nakamura, and S. Uchida, *Nature* **375,** 561 (1995).
35. S. Mori and C. K. Cheong, *Nature* **392,** 473 (1998).
36. S. Descurtins, P. Gütlich, C. Köhler, H. Spiering, and A. Hauser, *Chem. Phys. Let.* **105,** 1 (1984).
37. H. Watanabe, *J. Phys. Soc. Jpn.* **12,** 515 (1957).
38. B. Buffat, G. Demazeau, M. Pouchard, J. M. Dance, and P. Hagenmuller, *J. Solid State Chem.* **50,** 33 (1983).
39. J. B. Goodenough, *Mater. Res. Bull.* **6,** 967 (1971).
40. R. H. Potze, G. A. Sawatzky, and M. Abbate, *Phys. Rev. B* **51,** 11501 (1995).
41. S. F. Matar, A. Villesuzanne, and M. Uhl, *J. Mater. Chem.* **6,** 1785 (1996).
42. B. C. H. Steele, *Solid State Ionics* **134,** 3 (2000).